Magnetic-field generation and electron-collimation analysis for propagating fast electron beams in overdense plasmas

Hong-bo Cai,[1,2,*] Shao-ping Zhu,[1] Mo Chen,[1] Si-zhong Wu,[1] X. T. He,[1,2,3] and Kunioki Mima[4,5]
[1]*Institute of Applied Physics and Computational Mathematics, Beijing 100094, People's Republic of China*
[2]*Center for Applied Physics and Technology, Peking University, Beijing 100871, People's Republic of China*
[3]*Institute for Fusion Theory and Simulation, Zhejiang University, Hangzhou 310027, People's Republic of China*
[4]*Institute of Laser Engineering, Osaka University, 2-6 Yamadaoka, Suita, Osaka 565-0871, Japan*
[5]*The Graduate School for the Creation of New Photonics Industries, 1955-1 Kurematsu, Nishiku, Hamamatsu, Sizuoka 431-1202, Japan*
(Received 19 November 2010; revised manuscript received 25 January 2011; published 17 March 2011)

An analytical fluid model is proposed for artificially collimating fast electron beams produced in the interaction of ultraintense laser pulses with specially engineered low-density-core–high-density-cladding structure targets. Since this theory clearly predicts the characteristics of the spontaneously generated magnetic field and its dependence on the plasma parameters of the targets transporting fast electrons, it is of substantial relevance to the target design for fast ignition. The theory also reveals that the rapid changing of the flow velocity of the background electrons in a transverse direction (perpendicular to the flow velocity) caused by the density jump dominates the generation of a spontaneous interface magnetic field for these kinds of targets. It is found that the spontaneously generated magnetic field reaches as high as 100 MG, which is large enough to collimate fast electron transport in overdense plasmas. This theory is also supported by numerical simulations performed using a two-dimensional particle-in-cell code. It is found that the simulation results agree well with the theoretical analysis.

DOI: 10.1103/PhysRevE.83.036408 PACS number(s): 52.57.Kk, 52.38.Kd, 52.65.Rr

I. INTRODUCTION

In the concept of fast ignition (FI) [1], a highly compressed deuterium-tritium pellet, with a density of ∼300 g/cc and a radius of ∼10–20 μm at its core, is ignited by a ∼10 ps, 10 kJ intense flux of MeV electrons (or ions). These high-energy particles are generated by the absorption of an intense petawatt (10^{15} W) laser, at the edge of the pellet, which is usually ∼50 μm away from the dense core [2]. In order to deliver enough energy (∼10 kJ) into the pellet in ∼10 ps, the ignition laser beam should reach the intensity of $I_0 \sim 10^{20}$ W/cm^2 if the coupling from the laser to the core plasma is about 20% for a well-collimated beam [3]. However, studies have shown that the electron divergence increases with the laser intensity [4,5]. Shadowgraphy and K_α imaging measurements revealed an electron beam divergence of half angle of half maximum larger than 50° [6]. Therefore, of particular importance is the possibility of collimating the fast electron beams with the size of the compressed core.

To date, several works have been done regarding the control of the divergence of fast electron beams [7–13]. Robinson *et al.*'s hybrid-Vlasov-Fokker-Planck simulations [8] have shown some promising results, where the fast electrons are collimated in targets exhibiting a high-resistivity-core–low-resistivity-cladding structure analogous to optical waveguides. Recent experiments have also demonstrated this electron collimation in targets with a resistivity boundary [9,13]. In these cases, the magnetic-field growth can be derived from Faraday's law and Ohm's law as [14,15]

$$\frac{\partial \mathbf{B}}{\partial t} = c[\eta \nabla \times \mathbf{j}_h + (\nabla \eta) \times \mathbf{j}_h],$$

where η is the resistivity and $\mathbf{j}_h$ is the fast electron current density. Furthermore, numerical simulations by Zhou *et al.* [11] and Wu *et al.* [12] showed that a low-density-core–high-density-cladding structure target can also generate a megagauss (MG) interface magnetic field, which collimates fast electrons even better. However, according to the above equation, the magnetic field generated from the gradient of resistivity and current density should cause divergence of an electron beam, instead of collimating a beam. Therefore, their results clearly indicate that in a low-density-core–high-density-cladding structure target, other mechanisms tend to be dominant for the generation of a magnetic field. Such a spontaneous magnetic field has been explained by several mechanisms, such as anomalous resistivity [12]. However, there still does not exist a well-established and satisfactory theory, in particular, for quantitatively predicting the magnetic field and modeling its dependence on the plasma parameters.

In this paper, an analytical model describing this scenario is presented. The model, describing a uniform fast electron beam propagating in a low-density-core–high-density-cladding structure target, shows clearly the formation of the background return current flow and the generation of the spontaneous magnetic field. The mechanisms governing the generation of the magnetic field are studied in detail. It is found that the spontaneous magnetic field peaks at the interface and evanesces exponentially into the inner target over a characteristic skin depth. It is also found that the maximum magnetic field at the interface is proportional to the fast electron current and is inversely proportional to the square root of the background electron density of the inner target. Two-dimensional particle-in-cell (PIC) simulations have been run to verify this model. It is shown that the simulation results are very consistent with the prediction of our analytical model.

*caihonb@yahoo.com.cn

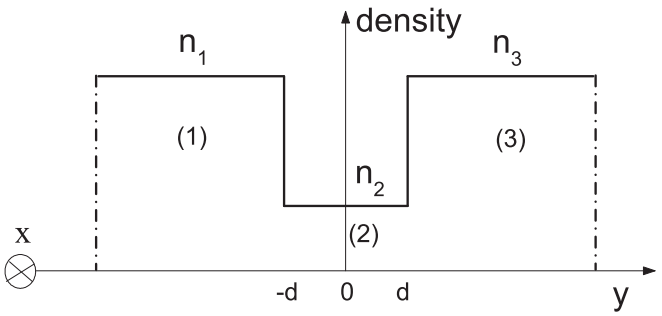

FIG. 1. Schematic of initial plasma density.

The paper is organized as follows. In Sec. II, the analytical model describing this scenario is studied in detail. In Sec. III, we present the PIC simulation for the generation of the magnetic field and the collimation of fast electron beams. In Sec. IV, a summary of the results is given.

II. ANALYTICAL DESCRIPTION OF THE SPONTANEOUSLY GENERATED MAGNETIC FIELD

We consider an ultraintense laser pulse with a large spot size normally irradiating on an unmagnetized low-density-core–high-density-cladding structure plasma with density profile as shown in Fig. 1, where ions form a fixed and neutralized background. A fast electron beam is generated at the laser plasma interface. If the spot size is large enough, we can simply assume that an equally infinite and uniform fast electron beam of density n_h propagates with an average velocity v_h along the x axis (longitudinal direction). The fast electron beam passing through the plasma quickly generates a return current of background thermal electrons. Suppose for a moment that the beam head is not neutralized by a balancing return current as the fast electron beam passes through the target. From the Maxwell equations, we get $\partial \mathbf{E}/\partial t = -4\pi \mathbf{j}_h$ [16]. The induced electric field is sufficiently strong to accelerate the background thermal electrons flowing in x direction with average velocity $v_{e0}(y)$.

For purpose of the interface magnetic-field excitation study, we assume that the fast electron beam motion is unperturbed. Since the magnetic field can develop in a very short time (of the order of a hundred femtoseconds), the combined system of the fast electron beam and the response of the background plasma can be suitably treated by a single fluid electron magnetohydrodynamic (EMHD) description. The EMHD equations, including electron-fluid equations and Maxwell equations, comprise a complete system of equations describing the electron response to the propagating fast beam pulse. The electron-fluid equations consist of the continuity equation

$$\frac{\partial n_e}{\partial t} + \nabla \cdot (n_e \mathbf{v}_{e0}) = 0, \tag{1}$$

and force balance equation

$$\frac{\partial \mathbf{p}_e}{\partial t} + (\mathbf{v}_{e0} \cdot \nabla)\mathbf{p}_e = -e\left(\mathbf{E} + \frac{1}{c}\mathbf{v}_{e0} \times \mathbf{B}\right) - \nabla P/n_e - \nu_{ei}\mathbf{p}_e, \tag{2}$$

where $-e$ is the electron charge, $\mathbf{v}_{e0}$ is the flow velocity of the background electrons, $\mathbf{p}_e = m_e\gamma_e\mathbf{v}_{e0}$ is the momentum of the background electrons, m_e is the electron rest mass, $\gamma_e = 1/\sqrt{1 - v_{e0}^2/c^2}$ is the relativistic factor, ∇P is the pressure gradient, and ν_{ei} is the e-i collision frequency. Eq. (2) can be simplified to

$$\frac{\partial(\mathbf{p}_e - \mathbf{a})}{\partial t} + \mathbf{v}_{e0} \times \nabla \times (\mathbf{p}_e - \mathbf{a}) = -\nabla\gamma_e + \nabla\phi - \nabla P/n_e - \nu_{ei}\mathbf{p}_e, \tag{3}$$

where $\mathbf{a}$ and ϕ are the vector and scalar potentials satisfying Coulomb gauge $\nabla \cdot \mathbf{a} = 0$. Operating on the electron momentum given by Eq. (3) with $\nabla\times$, we obtain the equation describing the transverse motion,

$$\frac{\partial \boldsymbol{\Omega}}{\partial t} + \mathbf{v}_{e0} \times \nabla \times \boldsymbol{\Omega} = \nabla n_e \times \nabla P/n_e^2 - \nabla \times (\nu_{ei}\mathbf{p}_e). \tag{4}$$

Here, $\boldsymbol{\Omega} = \nabla \times \mathbf{p_e} - e\mathbf{B}/c$ is the generalized vorticity. In the present study, due to the fast motion of the fast electron beam through the plasma, a flow in the return current is generated in the plasma with the flow velocity much faster than the electron thermal velocity. In such cases the electron pressure term can be neglected, in contrast to the case of slow beam pulses. Furthermore, there is no resistivity in the collisionless case ($\nu_{ei} = 0$). Therefore, vorticity is conserved [17–19]. If, before the arrival of the beam, we have $\nabla \times \mathbf{p_e} = 0$ and $\mathbf{B} = 0$, then $\boldsymbol{\Omega}(t = 0) = 0$. Eq. (4) then tells us that $\boldsymbol{\Omega} = 0$ for all time, so we can immediately write [20–23]

$$\mathbf{B} = \frac{c}{e}\nabla \times \mathbf{p_e}. \tag{5}$$

Similar processes have been discussed in Refs. [21–23]. This results in the relation $\frac{dv_{e0}}{dy} = -\frac{eB_0(y)}{m_e c}$ for the nonrelativistic case in the present study. Maxwell equations for the self-generated electric and magnetic fields, $\mathbf{E}$ and $\mathbf{B}$, are given by

$$\nabla \times \mathbf{B} = \frac{4\pi}{c}(-en_e\mathbf{p}_e/m_e\gamma_e + \mathbf{j}_h) + \frac{1}{c}\frac{\partial \mathbf{E}}{\partial t}. \tag{6}$$

Here, for a long beam with pulse length $l_b \gg v_h/\omega_p$, where v_h and ω_p are the fast electron beam velocity and background plasma frequency, the displacement current $\frac{1}{c}\frac{\partial \mathbf{E}}{\partial t}$ is of the order of $(v_h/\omega_p l_b)^2 \ll 1$ compared to the electron current. Therefore, in the following discussion, the displacement current is neglected [15,16,23]. Eq. (6) gives

$$\mathbf{p}_e = -\frac{m_e c\gamma_e}{4\pi e n_e}\nabla \times \mathbf{B} + m_e\gamma_e\mathbf{j}_h/en_e. \tag{7}$$

Substituting Eq. (7) into Eq. (5), we obtain the equation for the self-generated magnetic field,

$$\frac{m_e c^2}{4\pi e^2}\nabla \times \left(\frac{\gamma_e \nabla \times \mathbf{B}}{n_e}\right) + \mathbf{B} = \frac{m_e c\gamma_e}{e^2}\left(\frac{1}{n_e}\nabla \times \mathbf{j}_h - \frac{1}{n_e^2}\nabla n_e \times \mathbf{j}_h\right). \tag{8}$$

Equation (8) shows clearly that, in a collisionless case, the source of the self-generated magnetic field is $\frac{m_e c\gamma_e}{e^2}(\frac{1}{n_e}\nabla \times \mathbf{j}_h - \frac{1}{n_e^2}\nabla n_e \times \mathbf{j}_h)$, which means a target with sharp radial density boundary should build up strong magnetic fields at the boundary between a low-density core and

high-density cladding, which act to collimate the flow of fast electrons. The mechanism for magnetic-field generation described here is distinct from magnetic-field generation arising from the baroclinic source ($\partial\mathbf{B}/\partial t \propto \nabla n \times \nabla T$), which requires a temperature gradient [24], and from the resistivity gradient($\frac{\partial \mathbf{B}}{\partial t} = c[\eta\nabla \times \mathbf{j_h} + (\nabla\eta) \times \mathbf{j_h}]$), which requires the collision [16]. The mechanism considered here needs the density gradient instead of the resistivity gradient. The first term on the right-hand side of Eq. (8) generates a magnetic field that pushes fast electrons toward regions of higher fast electron current density, while the second term pushes fast electrons toward regions of lower density. It is not easy to solve Eq. (8) directly, even though Eq. (8) shows the physics clearly. However, we can still derive the magnetic field from Eqs. (5) and (7). Operating on Eq. (5) with $\nabla\times$, and substituting it into Eq. (7), we obtain

$$\frac{m_e c^2}{4\pi e^2}\frac{d^2 v_{e0}(y)}{dy^2} = n_e v_{e0}(y) + n_h v_h. \tag{9}$$

In the present case, the low-density-core–high-density-cladding structure background plasma has three different regions with ion densities as follows: n_{i1} for region 1 with $y < -d$, n_{i2} for region 2 with $-d \leqslant y \leqslant d$, and n_{i3} for region 3 with $y > d$, as shown in Fig. 1. Since the fast electron beam may be affected by this background plasma, we assume the densities of the fast electron beams for regions 1, 2, and 3 are n_{h1}, n_{h2}, and n_{h3}, respectively. Therefore, we can rewrite Eq. (9) as

$$\begin{aligned}
\left[\delta_{pe1}^2\frac{d^2}{dy^2} - 1\right]v_{e0} &= \frac{n_{h1}}{n_1}v_{h1}, \quad y < -d,\\
\left[\delta_{pe2}^2\frac{d^2}{dy^2} - 1\right]v_{e0} &= \frac{n_{h2}}{n_2}v_{h2}, \quad -d \leqslant y \leqslant d\\
\left[\delta_{pe3}^2\frac{d^2}{dy^2} - 1\right]v_{e0} &= \frac{n_{h3}}{n_3}v_{h3}, \quad y > d,
\end{aligned} \tag{10}$$

where $\delta_{pej} = c/\omega_{pej}$ $(j = 1, 2, 3)$ is the collisionless electron skin depth and $\omega_{pej} = \sqrt{4\pi n_j e^2/m_e}$ $(j = 1, 2, 3)$ is the electron plasma frequency for the background plasma in the jth region. Charge neutrality requires that $n_j = Z_j n_{ij} - n_{hj}$ $(j = 1, 2, 3)$, where n_j is the background thermal electron density and Z_j is the charge state for the jth region. That is to say, some of the thermal electrons will be expelled out of the regions where fast electrons arrive. We will discuss this physical process in detail in the next section. From Eq. (10), the flow velocity of the background thermal electrons can be solved analytically as follows:

$$v_{e0}(y) = \begin{cases} c_1\exp[(y+d)/\delta_{pe1}] - n_{h1}v_{h1}/n_1, & y < -d,\\ c_2\exp(-y/\delta_{pe2}) + c_3\exp(y/\delta_{pe2}) - n_{h2}v_{h2}/n_2, & -d \leqslant y \leqslant d\\ c_4\exp[-(y-d)/\delta_{pe3}] - n_{h3}v_{h3}/n_3, & y > d \end{cases} \tag{11}$$

The constants c_1, c_2, c_3,and c_4 can be determined from the boundary conditions:

$$\begin{aligned}
c_1 &= \frac{\delta_{pe1}}{\delta_{pe2}}\frac{\alpha_2\beta_1 + \alpha_1\beta_2\exp(2d/\delta_{pe2}) - \alpha_1\exp(-2d/\delta_{pe2}) - \alpha_2}{\beta_1\exp(-2d/\delta_{pe2}) - \beta_2\exp(2d/\delta_{pe2})},\\
c_2 &= -\frac{\alpha_2\beta_1\exp(-d/\delta_{pe2}) + \alpha_1\beta_2\exp(d/\delta_{pe2})}{\beta_1\exp(-2d/\delta_{pe2}) - \beta_2\exp(2d/\delta_{pe2})},\\
c_3 &= -\frac{\alpha_1\exp(-d/\delta_{pe2}) + \alpha_2\exp(d/\delta_{pe2})}{\beta_1\exp(-2d/\delta_{pe2}) - \beta_2\exp(2d/\delta_{pe2})},\\
c_4 &= \frac{\delta_{pe3}}{\delta_{pe2}}\frac{-\alpha_1\beta_2 - \alpha_2\beta_1\exp(-2d/\delta_{pe2}) + \alpha_1 + \alpha_2\exp(2d/\delta_{pe2})}{\beta_1\exp(-2d/\delta_{pe2}) - \beta_2\exp(2d/\delta_{pe2})},
\end{aligned}$$

where

$$\alpha_1 = \frac{\frac{n_{h2}v_{h2}}{n_2} - \frac{n_{h1}v_{h1}}{n_1}}{\frac{\delta_{pe1}}{\delta_{pe2}} + 1}, \quad \alpha_2 = \frac{\frac{n_{h2}v_{h2}}{n_2} - \frac{n_{h3}v_{h3}}{n_3}}{\frac{\delta_{pe3}}{\delta_{pe2}} - 1}, \quad \beta_1 = \frac{\delta_{pe1} - \delta_{pe2}}{\delta_{pe1} + \delta_{pe2}}, \quad \text{and} \quad \beta_2 = \frac{\delta_{pe3} + \delta_{pe2}}{\delta_{pe3} - \delta_{pe2}}.$$

Substituting Eq. (11) into Eq. (5) gives

$$\frac{eB_0}{m_e c} = -\frac{dv_{e0}(y)}{dy} = \begin{cases} -\frac{c_1}{\delta_{pe1}}\exp[(y+d)/\delta_{pe1}], & y < -d\\ \frac{1}{\delta_{pe2}}[c_2\exp(-y/\delta_{pe2}) - c_3\exp(y/\delta_{pe2})], & -d \leqslant y \leqslant d,\\ \frac{c_4}{\delta_{pe3}}\exp[-(y-d)/\delta_{pe3}], & y > d. \end{cases} \tag{12}$$

Equations (11) and (12) describe the background electron flow velocity and the spontaneous magnetic field. For simplicity, we assume a symmetric low-density-core–high-density-cladding structure target, which gives $n_1 = n_3$, $n_{h1} = n_{h3}$, and $v_{h1} = v_{h3}$. Furthermore, since the lower density region is much thicker than the skin depth $d \gg \delta_{pe2}$, it allows us to neglect the terms

with $\exp(-d/\delta_{pe2})$. Therefore, we can simplify the constants as follows: $c_1 = c_4 = \frac{\delta_{pe1}}{\delta_{pe1}+\delta_{pe2}}(\frac{n_{h2}v_{h2}}{n_2} - \frac{n_{h1}v_{h1}}{n_1})$ and $c_2 = c_3 = \frac{\delta_{pe2}}{\delta_{pe1}+\delta_{pe2}}(\frac{n_{h2}v_{h2}}{n_2} - \frac{n_{h1}v_{h1}}{n_1})\exp(-d/\delta_{pe2})$. Using Eq. (12), we obtain

$$\frac{eB_0}{m_e c} = \begin{cases} \frac{-1}{(\delta_{pe1}+\delta_{pe2})}\left(\frac{n_{h2}v_{h2}}{n_2} - \frac{n_{h1}v_{h1}}{n_1}\right)\exp\left[\frac{y+d}{\delta_{pe1}}\right], & y < -d, \\ \frac{1}{(\delta_{pe1}+\delta_{pe2})}\left(\frac{n_{h2}v_{h2}}{n_2} - \frac{n_{h1}v_{h1}}{n_1}\right)\left\{\exp[-\frac{y+d}{\delta_{pe2}}] - \exp[\frac{y-d}{\delta_{pe2}}]\right\}, & -d \leqslant y \leqslant d, \\ \frac{1}{(\delta_{pe1}+\delta_{pe2})}\left(\frac{n_{h2}v_{h2}}{n_2} - \frac{n_{h1}v_{h1}}{n_1}\right)\exp\left[-\frac{y-d}{\delta_{pe1}}\right], & y > d. \end{cases} \quad (13)$$

Figure 2 shows the schematic of the background electron flow velocity and the spontaneous magnetic field. It is evident in Fig. 2 that, for this kind of low-density-core–high-density-cladding structure target, the fast electron current is neutralized by the return current of thermal electrons everywhere except at the interfaces of different density regions over a characteristic transverse distance $\Delta y_\perp = \delta_{pe}$ [20]. Hence, the spontaneous magnetic field B_0 exists within a layer of width δ_{pe} near the interfaces of different regions, $y = \pm d$. We notice that B_0 peaks at the interface and evanesces exponentially to both sides over the skin depth. Since the skin depth is $\delta_{pe} \propto n_e^{-1}$ in the lower density plasma region, the magnetic field tunnels much deeper into the region, as shown in Fig. 2. For the case $n_1 \gg n_2$, Eq. (13) gives the maximum spontaneous magnetic field

$$B_{\max} \approx \frac{m_e\omega_0}{en_c}\frac{n_{h2}v_{h2}}{\sqrt{n_2/n_c}} \simeq 200\frac{\eta}{f}\frac{I_{18}^{1/2}\lambda_{\mu m}}{[(Z_2n_{i2}-n_{h2})/n_c]^{1/2}}\frac{v_{h2}}{c} \quad \text{MG.} \quad (14)$$

Here, the density of fast electrons required to carry the energy flux has been approximated by $n_{h2} \simeq \frac{2\eta}{f}(I_{18}\lambda_{\mu m}^2)^{1/2}n_c$ [16]. At these high intensities, we have approximated $2\eta/f \simeq 1/\sqrt{2}$. Equation (14) means that the magnitude of the magnetic field is strongly related to the incident laser intensity and the background electron density of the low-density core. This provides an interesting study when experiments begin to enter this regime. As a numerical example, we evaluate Eq. (14) for the case of the low-density-core–high-density-cladding structure target with $Z_1n_{i1} = Z_3n_{i3} = 200n_c$ and $Z_2n_{i2} = 10n_c$, irradiated by a laser light with $I\lambda_0^2 = 1.5 \times 10^{19}$ W/cm^{-2} μm^2, and assume $n_{h2} \approx 3n_c$ and $v_{h2} \sim c$ to obtain the qualitative estimate of the maximum magnetic field at the interface, $B_{\max} \approx$ 110 MG.

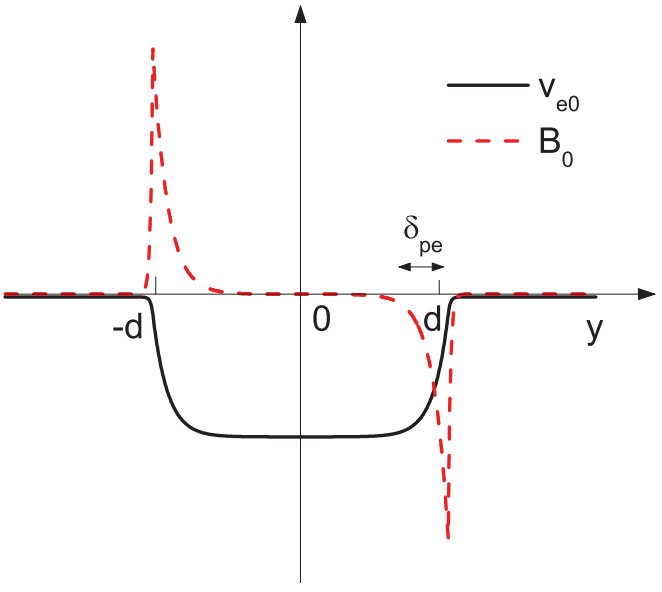

FIG. 2. (Color online) Schematic of the profile of the background electron flow velocity $v_{e0}(y)$ and the spontaneous magnetic field $B_0(y)$.

It is worth stressing that no significant contribution of the fast electron beam in the cladding regions (regions 1 and 3) to the magnetic field has been found. In other words, there is not much difference between the cases irradiating with a very large spot size laser and a finite spot size laser. In the case with a finite laser spot size, fast electron flow in region 1 and region 3 may be very weak, $n_{h1} = n_{h3} \approx 0$. From Eqs. (13) and (14), we can see that the magnetic field is only slightly influenced.

This simple analytical model is helpful for gaining insight into certain aspects of the generation of a spontaneous magnetic field and collimation of electron beams when fast electron beams propagate in a well-engineered low-density-core–high-density-cladding structure target. Unfortunately, the vast majority of experiments are inherently more complex, and these complications must be accounted for if a proper analysis of the physical process is to be done. The first, and most important, complexity we will discuss is that of the potential of beam-plasma instabilities. For this case, PIC simulation is a powerful tool to study it further.

III. NUMERICAL STUDY OF THE GENERATION OF A MAGNETIC FIELD

In order to describe the generation of magnetic fields in more detail, first we study low-density-core–high-density-cladding structure targets with the 2D3V (two spatial and three velocity components) PIC code ASCENT [25]. Figure 3 is a sketch of the geometry of the simulations. Regions 1 and 3 are fully ionized carbon (charge state $Z_i = 6$), with $m_i/m_eZ_i = 1836 \times 12/6$. Region 2 is the low-density hydrogen plasma. The widths of the three regions are $8.4\lambda_0$, $7.2\lambda_0$, and $8.4\lambda_0$, respectively. The densities of the three regions are $200n_c$, $5n_c$, and $200n_c$, respectively. In order to avoid ruining the hydrogen plasma by the laser pressure, we place another high-density target ($40n_c$) in front of the low-density-core–high-density-cladding structure target. The p-polarized laser pulse at $\lambda_0 = 1.06$ μm wavelength and 1.5×10^{19} W/cm^2 intensity irradiates the target from the left boundary. The

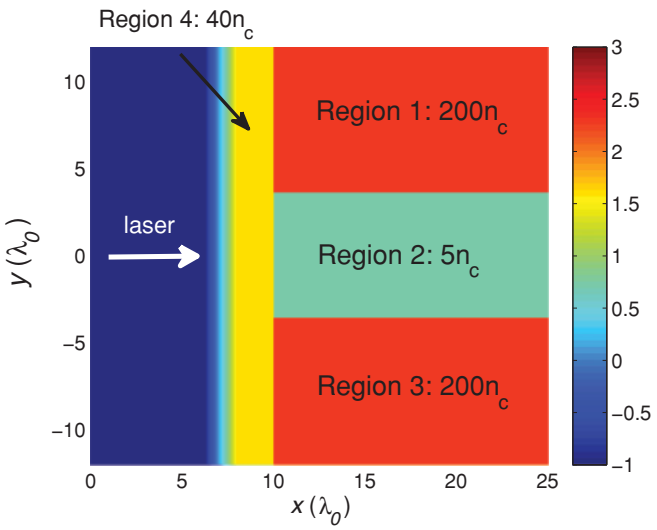

FIG. 3. (Color online) The initial density profile of the low-density-core–high-density-cladding structure target on a logarithmic scale.

intensity profile is Gaussian in the y direction with a spot size of 5.0 μm (full width at half maximum). The laser rises in $15T_0$, where T_0 is the laser period, after which the laser amplitude is kept constant.

The size of the simulation box is $30\lambda_0 \times 24\lambda_0$. Here, we use 3840×3072 grid cells with a grid size of $\Delta x = \Delta y = \lambda_0/128$. The time step used is $0.005T_0$, where T_0 denotes the laser period and its value is 3.3 fs for a 1.05-μm laser wave. During the simulation, we set 49 electrons and 49 ions per cell. The total number of particles is about 7.5×10^8. For both the fields and particles, we use the absorbing boundary condition in both x and y directions. Furthermore, in order to reduce the restrictions on the grid size compared with the Debye length, we use a fourth-order interpolation scheme to evaluate the fields and current [25]. In order to avoid the reflux of fast electrons, we set cooling buffers at the boundaries in our simulation.

Figure 4(a) shows the spontaneous magnetic field at time $t = 500$ fs. Clearly, a very large magnetic field has been generated at the interfaces, which plays a role in collimating fast electrons. Moreover, we observe that there are several

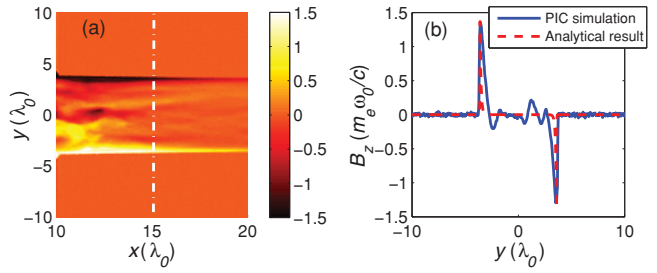

FIG. 4. (Color online) (a) The spontaneous magnetic fields at time $t = 500$ fs. (b) A slice of spontaneous magnetic fields at $x = 15\lambda_0$; the solid line is for the simulation result and the dash-dotted line is for the analytical result. Here, the magnetic fields are averaged over one laser period. The units of the magnetic field are $m_e\omega_0 c/e$ (1 unit = 100 MG).

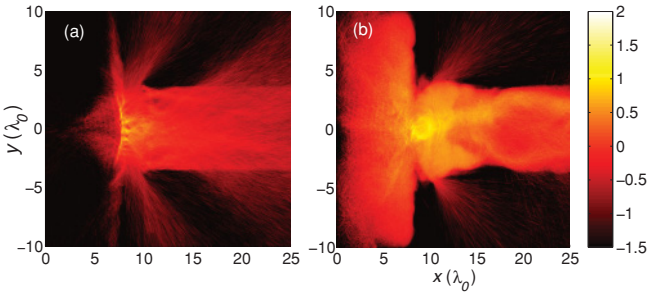

FIG. 5. (Color online) The electron energy density on a logarithmic scale at two different times, (a) $t = 264$ fs, and (b) $t = 1000$ fs. Here the electron energy density is normalized by $m_e c^2 n_c$.

stronger magnetic peaks in the inner target. These peaks are due to the formation of filament due to the Weibel instability [26]. Figure 4(b) shows a slice of spontaneous magnetic fields at $x = 15\lambda_0$; the solid line is for the simulation result and the dashed line is for the analytical result. We can see that the analytical result is consistent with the simulation result. However, the magnetic field is larger at the lower x position [as shown in Fig. 4(a)]. This is due to the complex beam-plasma instabilities (not only due to the present mechanism). At the position $x = 15\lambda_0$, the instabilities are still not developed, while the magnetic field is well developed. That is the reason why we choose to compare the analytical results with the simulated results at $x = 15\lambda_0$ or nearby. It should be noted that the suggested model is not enough to actually solve the two stream and Weibel instabilities, yet that is not the purpose of our study. Indeed, we focus on whether the interface magnetic field will develop when there is a forward fast electron beam passing the interfaces. Remarkably though, our explanation of why the 100 MG interface magnetic fields at the interfaces are generated applies to the self-consistent problem just as well.

We next examine how the spontaneous magnetic fields affect the transport of fast electron beams. In Fig. 5 the energy density distributions of electrons with energy between $0.5 \leqslant E_e \leqslant 5.0$ MeV are plotted. It is clearly seen that the fast electrons generated at the laser plasma interface have a large divergence angle. As time goes on, the electrons are highly collimated after the generation of the magnetic field, and few electrons can "leak" out into the high-density cladding.

For the fast electron beam with currents greater than the Alfvén limit, a return current moving in the opposite direction establishes approximately a charge- and current-neutral equilibrium [11,27]. Our theoretical model in Sec. II is quasineutral in both charge density and current density at the regions, except for the interfaces. Now we show how the neutralization is established. Figure 6 shows that, for electrons with energy between 1 and 50 keV [subplot (a)], and 100 and 5000 keV [subplot (b)], the mass current density extends from the layer of interaction is $\sim 7\lambda_0$ up to $25\lambda_0$ inside the plasma. This mass current density is superimposed on the structure of the spontaneous magnetic field that is mostly concentrated in the interaction region and low-density-core region. The peak value of the magnetic field is over 100 MG, which acts to collimate forward fast electrons and to scatter the returned

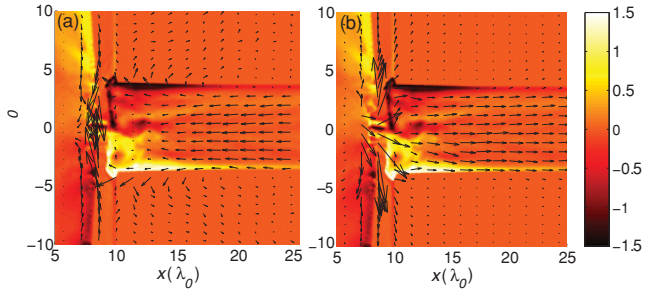

FIG. 6. (Color online) The mass flow of electrons at time $t =$ 500 fs with different energies (a) $E = (1,50)$ keV and (b) $E =$ (100,5000) keV. This mass flow is superimposed on the spontaneous magnetic field at $t = 500$ fs. The units of the magnetic field are $m_e\omega_0 c/e$ (1 unit = 100 MG).

background electrons. Figure 6(a) shows clearly that some return electrons are scattered out of the low-density-core region to keep the charge neutralization. Meanwhile, the returned background electrons are accelerated to higher velocity to maintain the current neutralization. Figure 6(b) shows that the fast electron beams are guided well by the magnetic field along the interface of the low-density-core region. It is also found in Fig. 6, when the fast electron pressure is developed, the inner interfaces of the plasmas of regions 1 and 3 are eroding, resulting in the outside expansion of the magnetic fields at the interfaces of the lower x position. However, such considerations are ignored in our simple model since the theory is developed in the framework of EMHDs.

IV. SUMMARY AND DISCUSSION

In summary, we have developed a self-consistent model to explore the generation mechanisms of a spontaneous magnetic field at the interfaces of a low-density-core–high-density-cladding structure target when a relativistic electron beam flows inside. The model revealed that the rapid changing of the flow velocity of the background electrons caused by the density jump dominates the generation of the spontaneous interface magnetic field for these kinds of targets. Our analytical results indicate that the magnetic field peaks at the interface, and evanesces exponentially into the inner region over a characteristic skin depth. It is found that the maximal magnetic field, which is proportional to the fast electron current and inverse proportional to the square root of the density of the inner region, can be as high as hundreds of megagauss. This should provide an interesting study for target design when experiments begin to enter this regime. It is also found that the fast electrons are collimated very well because of this magnetic field. These processes are verified with 2D3V PIC simulations.

While the generation of a spontaneous magnetic field at the interface of a low-density-core–high-density-cladding structure target and the collimation of fast electrons have been studied here in detail, the lifetime of this kind of target during the implosion compression in a fast ignition scenario still needs further study. In this scenario, radiation hydrodynamic code is needed to further study the implosion physics.

ACKNOWLEDGMENTS

We gratefully acknowledge C. Y. Zheng, L. H. Cao, Z. J. Liu, H. Nagatomo, T. Johzaki, and A. Sunahara for fruitful discussions. This work was supported by the National Natural Science Foundation of China (Grants No. 11045001, No. 11005011, No. 10835003, and No. 10935003), National Basic Research Program of China (973 Programs No. 2011CB808104, No. 2007CB814802) and the National High-Tech ICF Committee of China.

[1] M. Tabak *et al.*, Phys. Plasmas **1**, 1626 (1994).
[2] C. Ren, M. Tzoufras, F. S. Tsung, W. B. Mori, S. Amorini, R. A. Fonseca, L. O. Silva, J. C. Adam, and A. Heron, Phys. Rev. Lett. **93**, 185004 (2004).
[3] S. Atzeni, A. Schiavi, J. J. Honrubia, X. Ribeyre, G. Schurtz, Ph. Nicolai, M. Olazabal-Loume, C. Bellei, R. G. Evans, and J. R. Davies, Phys. Plasmas **15**, 056311 (2008).
[4] A. Debayle, J. J. Honrubia, E. d'Humieres, and V. T. Tikhonchuk, Phys. Rev. E **82**, 036405 (2010).
[5] K. L. Lancaster, J. S. Green, D. S. Hey, K. U. Akli, J. R. Davies, R. J. Clarke, R. R. Freeman, H. Habara, M. H. Key, R. Kodama, K. Krushelnick, C. D. Murphy, M. Nakatsutsumi, P. Simpson, R. Stephens, C. Stoeckl, T. Yabuuchi, M. Zepf, and P. A. Norreys, Phys. Rev. Lett. **98**, 125002 (2007).
[6] J. S. Green, V. M. Ovchinnikov, R. G. Evans, K. U. Akli, H. Azechi, F. N. Beg, C. Bellei, R. R. Freeman, H. Habara, R. Heathcote, M. H. Key, J. A. King, K. L. Lancaster, N. C. Lopes, T. Ma, A. J. Mackinnon, K. Markey, A. McPhee, Z. Najmudin, P. Nilson, R. Onofrei, R. Stephens, K. Takeda, K. A. Tanaka, W. Theobald, T. Tanimoto, J. Waugh, L. Van Woerkom, N. C. Woolsey, M. Zepf, J. R. Davies, and P. A. Norreys, Phys. Rev. Lett. **100**, 015003 (2008).
[7] J. A. King, K. U. Akli, R. R. Freeman, J. Green, S. P. Hatchett, D. Hey, P. Jamangi, M. H. Key, J. Koch, K. L. Lancaster, T. Ma, A. J. MacKinnon, A. MacPhee, P. A. Norreys, P. K. Patel, T. Phillips, R. B. Stephens, W. Theobald, R. P. J. Town, L. Van Woerkom, B. Zhang, and F. N. Beg, Phys. Plasmas **16**, 020701 (2009).
[8] A. P. L. Robinson, M. Sherlock, and P. A. Norreys, Phys. Rev. Lett. **100**, 025002 (2008); A. P. L. Robinson and M. Sherlock, Phys. Plasmas **14**, 083105 (2007).
[9] S. Kar, A. P. L. Robinson, D. C. Carroll, O. Lundh, K. Markey, P. McKenna, P. Norreys, and M. Zepf, Phys. Rev. Lett. **102**, 055001 (2009).
[10] M. Borghesi, A. J. Mackinnon, A. R. Bell, G. Malka, C. Vickers, O. Willi, J. R. Davies, A. Pukhov, and J. Meyer-ter-Vehn, Phys. Rev. Lett. **83**, 4309 (1999).
[11] C. T. Zhou *et al.*, Phys. Plasmas **17**, 083103 (2010); **15**, 123105 (2008); **92**, 071502 (2008); **92**, 151502 (2008); **97**, 201502 (2010).
[12] S. Z. Wu, C. T. Zhou, and S. P. Zhu, Phys. Plasmas **17**, 063103 (2010).
[13] B. Ramakrishna, S. Kar, A. P. L. Robinson, D. J. Adams, K. Markey, M. N. Quinn, X. H. Yuan, P. McKenna, K. L.

Lancaster, J. S. Green, R. H. H. Scott, P. A. Norreys, J. Schreiber, and M. Zepf, Phys. Rev. Lett. **105**, 135001 (2010).
[14] A. R. Bell, J. R. Davies, and S. M. Guerin, Phys. Rev. E **58**, 2471 (1998).
[15] J. R. Davies, Phys. Rev. E **68**, 056404 (2003).
[16] A. B. Bell, A. P. L. Robinson, M. Sherlock, R. J. Kingham, and W. Rozmus, Plasma Phys. **48**, R37 (2006).
[17] L. M. Gorbunov, P. Mora, and T. M. Antonsen Jr., Phys. Plasmas **4**, 4358 (1997).
[18] P. Gibbon, *Short Pulse Laser Interactions with Matter* (Imperial College Press, London, 2005).
[19] B. Qiao, X. T. He, and S. P. Zhu, Europhys. Lett. **72**, 955 (2005).
[20] E. A. Startsev, R. C. Davidson, and M. Dorf, Phys. Plasmas **16**, 092101 (2009).
[21] I. D. Kaganovich, E. A. Startsev, A. B. Sefkow, and R. C. Davidson, Phys. Rev. Lett. **99**, 235002 (2007); I. D. Kaganovich, G. Shvets, E. A. Startsev, and R. C. Davidson, Phys. Plasmas **8**, 4180 (2001).
[22] I. D. Kaganovich, E. A. Startsev, and R. C. Davidson, Phys. Plasmas **11**, 3546 (2004); I. D. Kaganovich *et al.*, *ibid.* **17**, 056703 (2010).
[23] I. D. Kaganovich, E. A. Startsev, A. B. Sefkow, and R. C. Davidson, Phys. Plasmas **15**, 103108 (2008).
[24] J. A. Stamper, K. Papadopoulos, R. N. Sudan, S. O. Dean, E. A. McLean, and J. M. Dawson, Phys. Rev. Lett. **26**, 1012 (1971).
[25] H. B. Cai, K. Mima, W. M. Zhou, T. Jozaki, H. Nagatomo, A. Sunahara, and R. J. Mason, Phys. Rev. Lett. **102**, 245001 (2009).
[26] F. Califano, D. Del Sarto, and F. Pegoraro, Phys. Rev. Lett. **96**, 105008 (2006).
[27] R. J. Mason, Phys. Rev. Lett. **96**, 035001 (2006).